JOURNAL OF GEOPHYSICAL RESEARCH, VOL. 113, D21308, doi:10.1029/2008JD009860, 2008

Seasonal persistence of northern low- and middle-latitude anomalies of ozone and other trace gases in the upper stratosphere

S. Tegtmeier,[1] V. E. Fioletov,[1] and T. G. Shepherd[2]

Received 23 January 2008; revised 10 July 2008; accepted 23 July 2008; published 11 November 2008.

[1] Analysis of observed ozone profiles in Northern Hemisphere low and middle latitudes reveals the seasonal persistence of ozone anomalies in both the lower and upper stratosphere. Principal component analysis is used to detect that above 16 hPa the persistence is strongest in the latitude band 15–45°N, while below 16 hPa the strongest persistence is found over 45–60°N. In both cases, ozone anomalies persist through the entire year from November to October. The persistence of ozone anomalies in the lower stratosphere is presumably related to the wintertime ozone buildup with subsequent photochemical relaxation through summer, as previously found for total ozone. The persistence in the upper stratosphere is more surprising, given the short lifetime of O_x at these altitudes. It is hypothesized that this "seasonal memory" in the upper stratospheric ozone anomalies arises from the seasonal persistence of transport-induced wintertime NO_y anomalies, which then perturb the ozone chemistry throughout the rest of the year. This hypothesis is confirmed by analysis of observations of NO_2, NO_x, and various long-lived trace gases in the upper stratosphere, which are found to exhibit the same seasonal persistence. Previous studies have attributed much of the year-to-year variability in wintertime extratropical upper stratospheric ozone to the Quasi-Biennial Oscillation (QBO) through transport-induced NO_y (and hence NO_2) anomalies but have not identified any statistical connection between the QBO and summertime ozone variability. Our results imply that through this "seasonal memory," the QBO has an asynchronous effect on ozone in the low to midlatitude upper stratosphere during summer and early autumn.

Citation: Tegtmeier, S., V. E. Fioletov, and T. G. Shepherd (2008), Seasonal persistence of northern low- and middle-latitude anomalies of ozone and other trace gases in the upper stratosphere, *J. Geophys. Res.*, *113*, D21308, doi:10.1029/2008JD009860.

1. Introduction

[2] During winter and early spring there is a buildup of total ozone in midlatitudes which is caused by the dominance of transport processes during this period. This buildup is followed by a decline through late spring and summer when transport becomes less important and photochemical loss controls the seasonal evolution of midlatitude total ozone. There is a significant amount of interannual variability in midlatitude total ozone, most notably in the winter and early spring buildup period. It is well established that the springtime total ozone anomalies are related to anomalies in the dynamical forcing of the Brewer-Dobson circulation [*Fusco and Salby*, 1999; *Randel et al.*, 2002; *Weber et al.*, 2003]. It is also well established that the quasi-biennial oscillation (QBO) in tropical zonal wind is one of the dominant influences on year-to-year variability in extratropical total ozone [e.g., *Hamilton*, 1989; *Gray and Dunkerton*, 1990; *Tung and Yang*, 1994; *Randel and Wu*, 1996]. The QBO affects extratropical ozone by modulating the extratropical planetary wave dynamics and hence the dynamical forcing of the Brewer-Dobson circulation [*Holton and Tan*, 1980]. Since planetary waves can only propagate into the extratropical stratosphere during the half of the year when the winds are westerly, the observed QBO signal in extratropical total ozone is synchronized with the annual cycle [e.g., *Tung and Yang*, 1994], with maxima in the winter-spring hemisphere.

[3] Long-term records of satellite ozone profile measurements make it possible to investigate the vertical structure of ozone anomalies. A boundary between dynamical and photochemical control of ozone around 16 hPa can be seen, for example, from analysis of the vertical structure of the QBO signal in ozone [*Zawodny and McCormick*, 1991; *Chipperfield et al.*, 1994; *Randel and Wu*, 1996]. In particular, the extratropical ozone QBO signal has a double peaked structure in the vertical with maxima in the lower (20–27 km) and middle/upper (30–37 km, with 16 hPa being near 30 km) stratosphere. The separation between the two partial ozone columns at 16 hPa is situated at a middle stratospheric level. To simplify matters we will refer to the partial ozone column below 16 hPa as ozone from the lower stratosphere and to the partial ozone column above 16 hPa as ozone from the upper stratosphere. On average, about 75% of the total ozone is found below 16 hPa in midlati-

[1] Environment Canada, Toronto, Ontario, Canada.
[2] Department of Physics, University of Toronto, Toronto, Ontario, Canada.

0148-0227/08/2008JD009860$09.00

tudes. In this lower stratospheric region O_x has a long lifetime (months to years) and ozone is mainly under dynamical control (apart from the influence of polar ozone loss). Year-to-year variations in lower stratospheric ozone peak in winter and early spring and are likewise dominated by variations in transport. Accordingly, the QBO signal in extratropical ozone in the lower stratosphere spans a wide latitude range from 15° to 60° [*Randel and Wu*, 1996].

[4] Above 16 hPa, on the other hand, O_x has a short lifetime and ozone is photochemically controlled [*Brasseur and Solomon*, 1984]. In this region the extratropical ozone QBO signal, which spans the latitude range from 10° to 40°, is understood to arise from QBO-induced variability in the transport of NO_y which affects ozone chemically through NO_2 [*Zawodny and McCormick*, 1991; *Chipperfield et al.*, 1994; *Randel and Wu*, 1996]. These QBO signals in ozone and NO_2, which reflect the instantaneous correlations of interannual anomalies, are especially strong in winter and early spring when the Brewer-Dobson circulation penetrates deep into the stratosphere and stratospheric transport can be modulated by the QBO. They are usually identified statistically under the assumption that the signals represent a smooth long-term fluctuation with the QBO period of about 28 months modulated by the 12 month seasonal cycle, using either digital filtering or Fourier analysis [*Tian et al.*, 2006] or regression with the equatorial wind [*Randel and Cobb*, 1994; *Randel and Wu*, 1996, 2007]. However, using regression methods the correlation between the equatorial wind and extratropical ozone in summer and autumn is small [*Randel and Wu*, 2007, Figure 14]. On the other hand, upper stratospheric ozone variability during summer and autumn is substantial [*Randel and Wu*, 1995]. In this study we show that ozone variations in the upper stratosphere over northern low and middle latitudes in summer and autumn are in fact related to those in winter and spring.

[5] *Fioletov and Shepherd* [2003, hereinafter referred to as FS 2003] showed that the interannual anomalies in midlatitude total ozone established in the winter-spring ozone buildup persist through summer until the ozone minimum in autumn. During the summertime period of total ozone decline the ozone anomalies decrease in magnitude through photochemical relaxation, and then are rapidly erased when the next winter's buildup begins. It is of interest to ask what the structure of this seasonal persistence might be as a function of altitude. Since transport-induced total ozone anomalies are mainly coming from the lower stratosphere, a similar persistence of anomalies for ozone in the lower stratosphere can be expected. In the upper stratosphere one might not expect much seasonal persistence because ozone is under photochemical control and the short lifetime of O_x precludes a transport-induced buildup of ozone anomalies during winter. Likewise, dynamically induced temperature fluctuations which would also affect upper stratospheric ozone (through changing the chemical loss rates) would be rapidly erased in early summer because of the short (several days) radiative time scale in this region. However, because of the effect of wintertime transport on the catalytic species like NO_2 (through the long-lived NO_y family), which as noted above is understood to be the mechanism for how the QBO affects extratropical upper stratospheric ozone during winter and early spring, it is reasonable to hypothesize that the springtime NO_2 anomalies would persist through the dynamically quiescent summer, analogous to the persistence of the lower stratospheric ozone anomalies. This seasonal persistence would influence ozone chemistry through the summer, and thereby provide an explanation for the ozone variations observed in the upper stratosphere in summer and autumn.

[6] In this study we therefore analyze the persistence of upper and lower stratospheric ozone anomalies over northern low and middle latitudes, as well as of upper stratospheric anomalies in other trace gases, using the same approach as FS 2003. Gaps in the data records make it more difficult to perform a similar analysis for the Southern Hemisphere. Ozone variations over the equatorial region are different from those over midlatitudes and will be the subject of a separate study. The data sets are described in section 2. Section 3 presents the results for ozone based on autocorrelation functions and principal component analysis (PCA). In section 4 the persistence of other trace gases is analyzed in order to test the hypothesis that the seasonal persistence in extratropical upper stratospheric ozone anomalies results from the persistence of transport-induced wintertime NO_y anomalies. A summary is provided in section 5.

2. Data Sets

[7] The estimation of autocorrelation functions requires a long-term time series of data. Such time series of ozone profile data are available from three satellite instrument systems: Solar Backscatter Ultraviolet instrument (SBUV, SBUV/2), Stratospheric Aerosol and Gas Experiment (SAGE), and Halogen Occultation Experiment (HALOE).

2.1. Merged SBUV(/2) Data Set

[8] The SBUV instrument was originally installed on Nimbus 7 and the subsequent SBUV/2 instruments were flown on the sequence of NOAA satellites (9, 11, 14, 16, 17, and 18). The SBUV(/2) data have been reprocessed recently with the new version 8 algorithm [*Bhartia et al.*, 2004]. The SBUV(/2) measurements provide nearly global daily coverage of the ozone distribution with a vertical resolution of about 5 km. Results of SBUV(/2) ozone profile comparisons with other data sources have demonstrated their good quality, although some problems with individual instrument records have also been reported [*Petropavlovskikh et al.*, 2005; *Nazaryan and McCormick*, 2005; *Fioletov et al.*, 2006; *Terao and Logan*, 2007].

[9] The merged SBUV(/2) profile ozone data set used in this study is prepared by NASA [*Frith and Stolarski*, 2005] on the basis of the SBUV version 8 algorithm (http://hyperion.gsfc.nasa.gov/Data_services/merged/mod_data.public.html). It is a set of monthly zonal mean values covering the time period from November 1978 to December 2007. Data from the BUV instrument on board the NOAA 4 satellite are also included in the merged data set. These data provide a nearly continuous record in 1970–1972, but there are only occasional observations in 1973–1977. The BUV data were not used for correlation function analysis, but they are included in the reconstructed ozone plots in section 5. The ozone profile data are given as partial total columns in Dobson Units (DU) for 13 layers, each 3.2 km thick except for layer 1, which is about 18 km. This study is

Table 1. Layers for SBUV(/2) Profile Ozone Data

Layer	Pressure (hPa)
1	1000–64
2	64–40
3	40–25
4	25–16
5	16–10
6	10–6
7	6–4
8	4–2.5
9	2.5–1.6

focused on layers 1 to 9 (Table 1). The monthly zonal mean ozone profiles are given in 5° wide latitude bands and cover up to 80°N from April to September and up to 60°N for the rest of the year. Because of the NOAA satellite orbits, the data in the latitude band 55°N to 60°N and in some years in the band 50°N to 55°N are missing for December and/or January for nine winters in recent years. These gaps are filled with the data from the adjacent latitude band at the lower latitude. The gaps due to the NOAA satellite orbits in the Southern Hemisphere are larger and latitudes as low as 35°S are affected. These gaps are one of the reasons why this study is limited to the Northern Hemisphere. In addition, the data for March 1991, August and September 1995, May and June 1996, July 1997 as well as May 1998 are missing since no reliable satellite data are available. Furthermore data are missing for 10°S to 30°N for the time period March 1982 to February 1983 following the eruption of El Chichon, and for 20°S to 30°N for the time period June 1991 to May 1992 following the eruption of Mt. Pinatubo.

2.2. SAGE II Data Set

[10] The SAGE measurement technique [*McCormick et al.*, 1989; *Zawodny and McCormick*, 1991] is based on solar occultation, with ozone profile measurements obtained at sunrise and sunset on each of 14 orbits per day. Spatial sampling is limited, and it takes approximately 1 month to sample the latitude range 60°N to 60°S. The ozone and nitrogen dioxide (NO_2) data from the SAGE II sensor aboard the Earth Radiation Budget Satellite (ERBS) for the period from January 1985 to December 2003 processed with the version 6.2 retrieval algorithm with an additional quality control [*Rind et al.*, 2005] are used here. The SAGE data products are presented on 16 standard pressure levels from 700 to 0.2 hPa. Zonal monthly means of the ozone volume mixing ratio and of the NO_2 volume mixing ratio given in 8° wide latitude bands between 55°S and 55°N are analyzed. NO_2 sunset observations only are used to avoid issues related to the systematic difference between sunrise and sunset concentrations. We focus on the pressure levels around 10 hPa over the northern midlatitudes. Because of the satellite orbit, data records there have substantial gaps in some individual months of the year. For ozone, the data gaps mainly occur from May until August and therefore only time series for the months between September and April can be used for the analysis. The sunset NO_2 measurements are even sparser with sufficiently long time series available only for November, January, February, March, and April.

2.3. HALOE Data Set

[11] The HALOE instrument [*Russell et al.*, 1993] aboard the Upper Atmosphere Research Satellite (UARS) observed mixing ratios of the trace gases CH_4, H_2O, HCl, HF, O_3, NO and NO_2 from 1991 to 2005. The measurements are based on the solar occultation technique with daily observations of up to 15 sunrise and 15 sunset profiles. The observations cover up to 80°N from April to September and up to 50°N for the rest of the year. The HALOE data set used in this study is prepared by *Grooβ and Russell* [2005]. It is a set of monthly mean values covering the time period from October 1991 to August 2002. The most recent data has not been included in this data set since the observations have been much less frequent after 2002. The data are averaged over 5° wide equivalent latitude bins. The mixing ratio profiles of the trace species are given for 22 pressure levels between 316 and 0.1 hPa. We focus in this study on CH_4, H_2O, HCl, HF, and NO_x at the pressure level 10 hPa over the northern midlatitudes. The NO_x profile is calculated as the sum of the measured NO and NO_2 and is based on sunset events only.

3. Short-Term Ozone Variations for Different Altitude Regions

3.1. Ozone Autocorrelation Functions

[12] Figure 1 shows the ozone seasonal cycle over 35–60°N for different years derived from the SBUV(/2) profile ozone data set. The ozone column between 1000 and 1.6 hPa (which we will refer to as the total ozone column), the partial ozone column between 1000 and 16 hPa (with 16 hPa being near 30 km), and the partial ozone column between 16 and 1.6 hPa (with 1.6 hPa being near 48 km) are plotted. The ozone seasonal cycle in the lower stratosphere (Figure 1b) shows a springtime maximum reflecting the buildup due to transport in winter and late spring, and subsequent photochemical loss in late spring and summer. This behavior is made possible by the lifetime of O_x in the lower stratosphere, which can be up to several years. The year-to-year variations are maximal in winter and early spring when they reach values of up to 60 DU, which corresponds to 20% of the partial ozone column. Figure 1c displays the seasonal cycle of ozone in the upper stratosphere, with high ozone values in summer and low ozone values in winter. This behavior is mainly due to the dependence of the Chapman mechanism on the intensity of shortwave radiation. The year-to-year variations are about 10 DU, which corresponds to 12% of the partial ozone column in the upper stratosphere. The seasonal cycle of the total ozone column (Figure 1a) is mainly explained by the seasonal cycle of ozone in the lower stratosphere, since this region contains most of the total ozone.

[13] Negative or positive ozone anomalies in individual years appear to persist during the displayed seasonal cycle for all three altitude regions. The persistence in total ozone was originally reported by FS 2003. It is related to the link between winter-spring ozone buildup due to transport and subsequent chemical loss in the dynamically quiescent summer stratosphere. Since transport-induced total ozone anomalies are mainly coming from the lower stratosphere, a similar persistence of anomalies for the total ozone column and for ozone in the lower stratosphere can be expected. The apparent persistence of the upper stratospheric anoma-

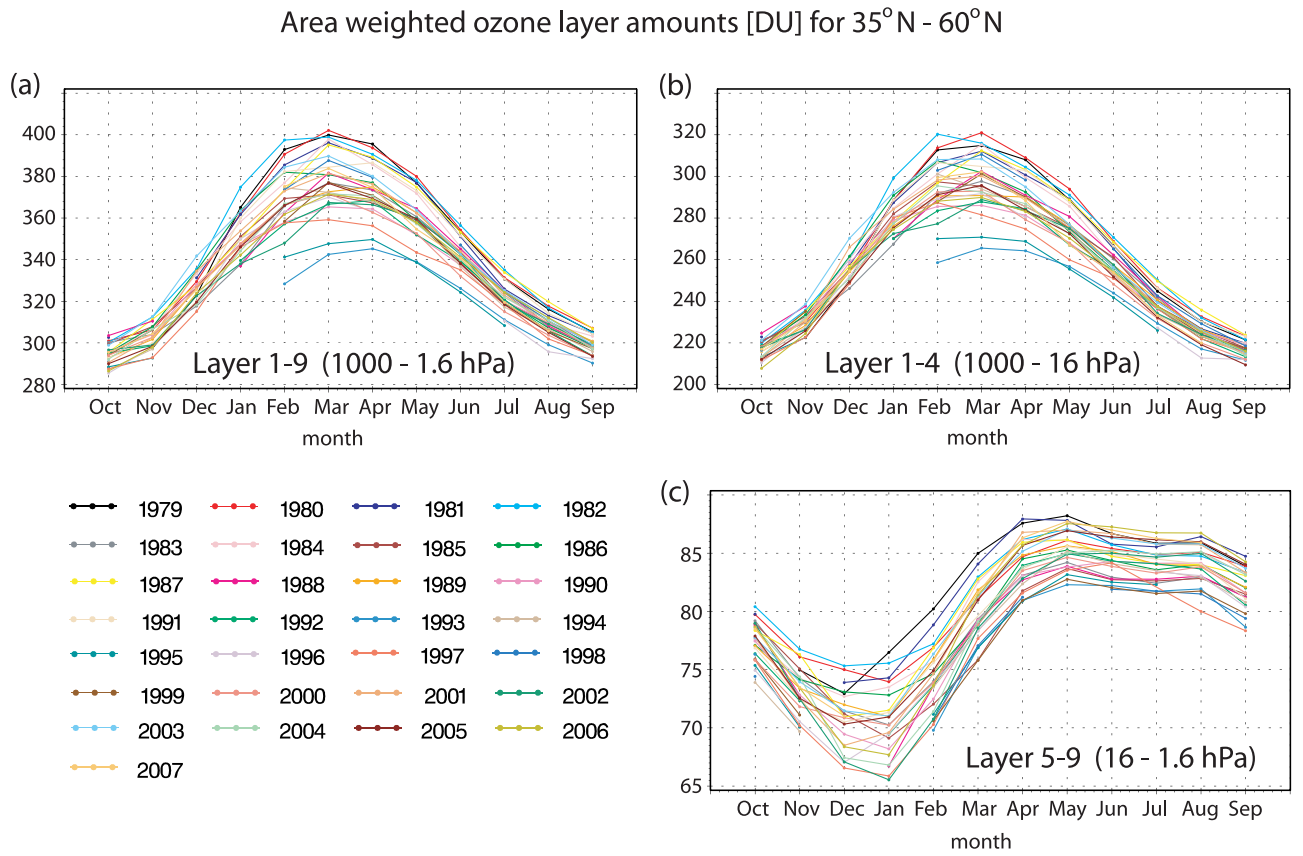

Figure 1. Seasonal cycle of area weighted ozone layer amounts averaged over 35–60°N for the merged SBUV(/2) profile ozone data for the ozone column (a) between 1000 and 1.6 hPa, (b) between 1000 and 16 hPa, and (c) between 16 and 1.6 hPa. Each curve corresponds to a different year, as labeled.

lies is more surprising, and is the main focus of this paper. We note for future reference that while the lower stratospheric anomalies decline in magnitude during the summer, the upper stratospheric anomalies do not.

[14] Following the FS 2003 approach, correlation functions between the time series of partial ozone columns for individual months are used to quantify the persistence of ozone anomalies. The long-term trend is removed from the original data prior to the correlation coefficient calculations. The equivalent effective stratospheric chlorine (EESC) loading is used as a proxy for the long-term trend, which is estimated separately for each month of the year for all latitude bands. The EESC function for the midlatitude lower stratosphere is used for all layers. While the EESC function for the upper stratosphere is slightly different from that for the lower stratosphere [*Newman et al.*, 2007], this difference has practically no effect on the correlation coefficients of the detrended data.

[15] We calculate ozone autocorrelations for partial ozone columns within certain latitude bands as a function of time lag for each month of the year. The autocorrelation is thus

$$R(t,\tau) = \frac{\sum_{i=1}^{n} f_i(t) f_i(t+\tau)}{\sqrt{\sum_{i=1}^{n} f_i(t)^2}\sqrt{\sum_{i=1}^{n} [f_i(t+\tau)]^2}}$$

where n is the number of years in the record, t is a particular month, $t+\tau$ is a subsequent month lagged by τ months, and f_i is the deviation from the mean in the year i. The correlation coefficients between SBUV(/2) ozone values for the same month in different years are low. Thus each year can be considered as independent. On the basis of the Student's t test, we find that correlation coefficients greater than 0.4 are then statistically significant at the 95% confidence level for this 25-year time series.

[16] Figure 2 shows the ozone autocorrelation functions for 35–60°N for different months of the year. As noted by FS 2003, the autocorrelations for total ozone (Figure 2a) decrease slowly during winter, spring and summer and then fall off sharply during autumn. This reflects the fact that there is not a great deal of dynamical variability in the late spring and summer stratosphere at midlatitudes. In the lower stratosphere (Figure 2b), the persistence of the ozone anomalies is similar to that observed for the total ozone column. Rather surprisingly, the pattern of autocorrelation functions in the upper stratosphere (Figure 2c) is very similar and the persistence of correlations is even slightly stronger compared to the pattern in the lower stratosphere and in the total ozone column.

[17] There is some correlation between partial column ozone retrieved by the SBUV(/2) instrument, particularly for adjacent layers, possibly caused by the observation method and retrieval algorithm. However, this vertical correlation is not enough to explain the persistence of upper stratospheric ozone anomalies from the persistence of lower stratospheric ozone anomalies, as the correlation coefficient

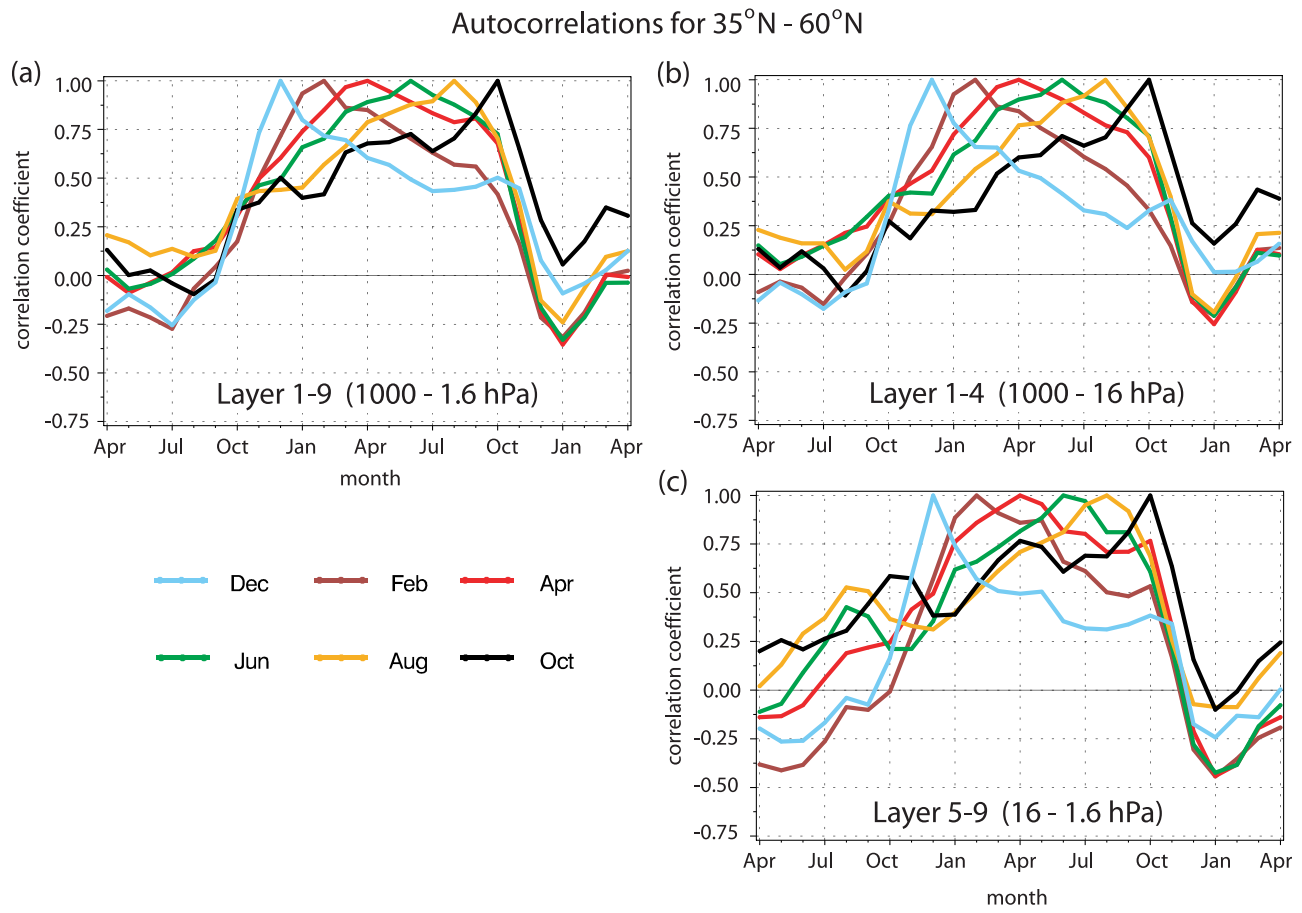

Figure 2. Ozone autocorrelation functions for the region 35–60°N for the merged SBUV(/2) profile ozone data for the ozone column (a) between 1000 and 1.6 hPa, (b) between 1000 and 16 hPa, and (c) between 16 and 1.6 hPa. Each curve represents the autocorrelation with respect to a particular month, as labeled.

between ozone anomalies in the lower stratosphere and in the upper stratosphere for 35–60°N is only about 0.4.

[18] While the patterns of autocorrelation functions for the lower and upper stratosphere covering the 35–60°N belt look very similar, this is not always the case for other latitude belts. In the following we enlarge the examined region to 15°N and split the whole subtropical/midlatitude region at 45°N. This choice is motivated by the results of instantaneous cross correlations between total ozone values at different latitude bands in *Fioletov and Shepherd* [2005]. The cross correlations for NH spring show a clear boundary at 45°N between two areas of high correlations, with the low-latitude cluster starting at 15°N. The autocorrelation functions for the latitude band 45–60°N show a clear clustered structure in the lower stratosphere (Figure 3a). In the upper stratosphere (Figure 3b) the correlations are less strong than in the lower stratosphere during winter and early spring, and of comparable strength in late spring and summer. The picture changes completely, however, if we look at adjacent bands at lower latitudes such as the latitude band 15–45°N. Now the ozone autocorrelation functions in the upper stratosphere (Figure 3d) show a clustered structure. The correlations are very high within 1 year from autumn to autumn of the next year. In the lower stratosphere the autocorrelations are much weaker and fall off quickly after 1 or 2 months (Figure 3c).

[19] The analysis of ozone anomalies based on autocorrelation functions was also applied to the SAGE II ozone data set. On the basis of the Student's *t* test, correlation coefficients greater than 0.45 are statistically significant at the 95% confidence level for the 19-year-long SAGE II time series. The persistence of ozone anomalies in the subtropical upper stratosphere, which was shown to be especially strong in the SBUV(/2) ozone data set, is of particular interest here. Figure 4 displays the autocorrelation functions for the ozone volume mixing ratio at 10 hPa for 15–45°N for different months of the year. The correlations between ozone in May, June, July and August and ozone in other months are not displayed because of data gaps in these 4 months. Nevertheless, for ease of comparison the ranges of the *x* and *y* axes have been chosen to be the same as in Figure 3. The autocorrelations from December until April show high values (greater than 0.75) and demonstrate that the SAGE II ozone anomalies persist during winter and early spring. They then fall off sharply in the next autumn. The SAGE II autocorrelations thus show a very similar behavior to the SBUV(/2) autocorrelations in the upper stratosphere in the region 15–45°N (Figure 3d), although they are not quite as strong during wintertime. This might be due to the limited

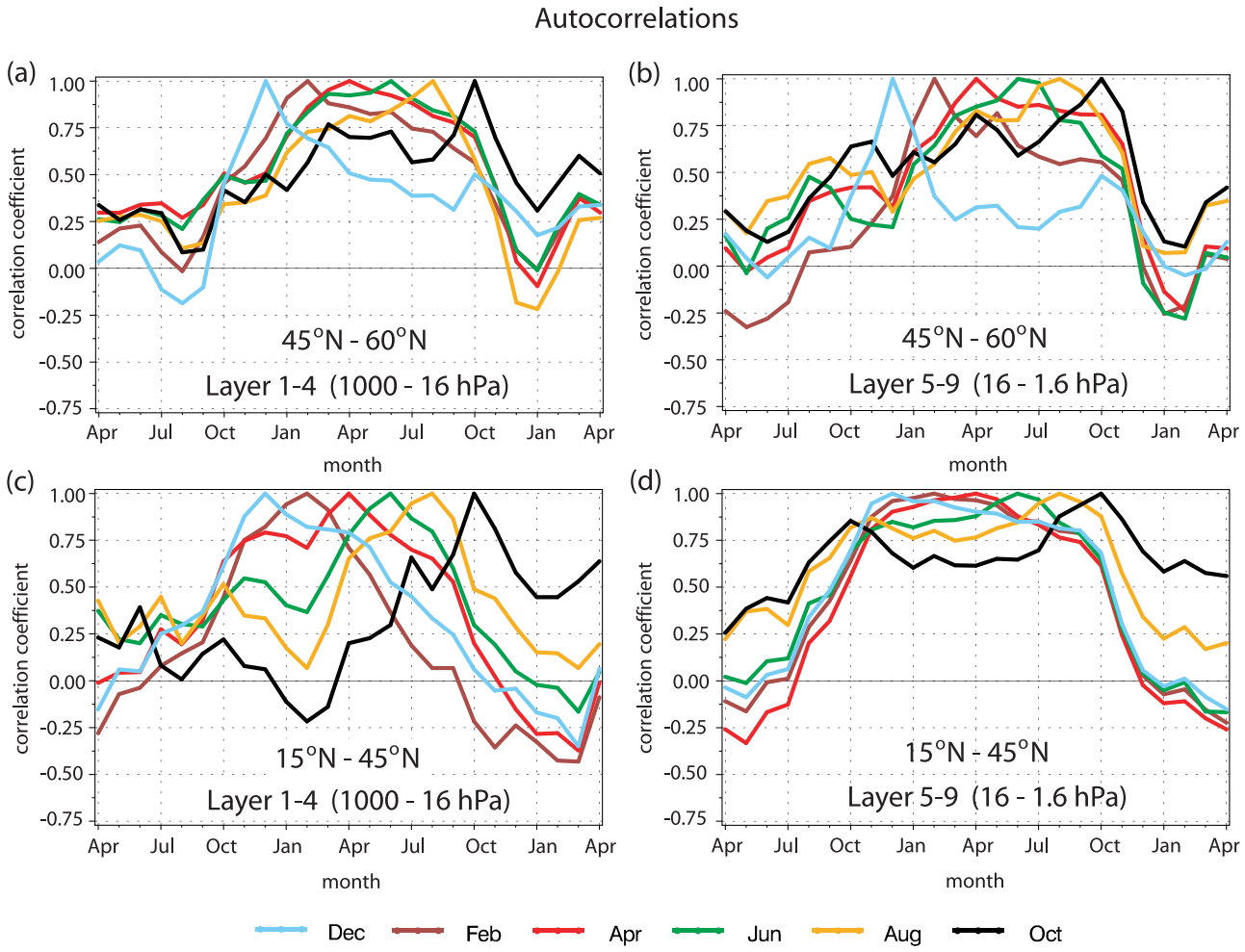

Figure 3. Ozone autocorrelation functions for the merged SBUV(/2) profile ozone data for the region 45–60°N for the ozone column (a) between 1000 and 16 hPa and (b) between 16 and 1.6 hPa and for the region 15–45°N for the ozone column (c) between 1000 and 16 hPa and (d) between 16 and 1.6 hPa. Each curve represents the autocorrelation with respect to a particular month, as labeled.

spatial coverage of the SAGE II data set. In general, however, the persistence of the SAGE II ozone anomalies confirms our observations made for the SBUV(/2) ozone profile data set.

3.2. Principal Component Analysis

[20] The ozone autocorrelation functions for the upper stratosphere from the two independent data sets SBUV(/2) and SAGE II show a clustered structure which for the 15–45°N belt starts in autumn and ends in autumn of the following year. This means that a substantial fraction of the ozone variability in different months can be "explained" by a single variable or "component." Such a component can be determined by principal component analysis (PCA) [*Richman*, 1986; *Preisendorfer*, 1988].

[21] The idea of PCA is to reduce a complex data set to a lower dimension to reveal a simplified underlying structure. The complex data set we are interested in consists of 12 variables which are the time series of SBUV(/2) ozone anomalies for 12 months, for example from October to September of the following year. PCA explains the 12 variables in terms of a much smaller number of variables, the so-called principal components. They are linear functions of the 12 original variables and can be derived from the eigenvectors of the corresponding correlation matrix sorted by decreasing values of the associated eigenvalues (see e.g., *Afifi and Azen* [1979] for details). We focus here on the first principal component, which corresponds to the first eigenvalue. The first principal component accounts for only a fraction of the variance of the whole underlying data set, which is equal to the first eigenvalue divided by the sum of all eigenvalues. Therefore a first eigenvalue close to the value 12 indicates that the first principal component accounts for most of the variance in our underlying data set, and means that the 12 time series of ozone anomalies are strongly correlated.

[22] To illustrate the relation between the 12 variables of the underlying data set and the first principal component, Figure 5a shows the detrended standardized (i.e., divided by the standard deviation) ozone anomalies for the individual months of the time frame starting in October and ending in September of the following year for the upper layers for the latitude band 15–45°N. Furthermore Figure 5a displays the corresponding first principal component, which shows

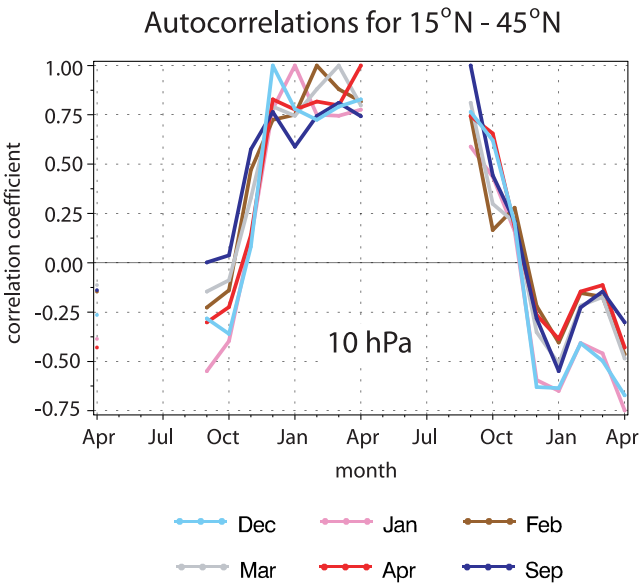

Figure 4. Ozone autocorrelation functions for the region 15–45°N for the SAGE II ozone data for the ozone volume mixing ratio at 10 hPa. Each curve represents the autocorrelation with respect to a particular month. The correlations between ozone in May, June, July, and August and ozone in other months are not displayed because of data gaps in these 4 months.

the same pattern of interannual variability as the individual time series of ozone anomalies. To keep the vertical scale the same for all data sets, the first principal component shown in the plot was also standardized. Figure 5b shows the 12 variables of the underlying data set and the first principal component for the latitude band 45–60°N. Here the patterns of interannual variability of the 12 ozone time series vary much more than for the latitude band 15–45°N. Therefore in this case the first principal component is less capable of representing the interannual variability of the whole underlying data set.

[23] The first eigenvalue for the latitude band 15–45°N (Figure 5a) is very high (10.13). This indicates that the first principal component provides a very good summary of the whole data set, accounting for 84.4% of its total variance. The data set for the midlatitude band 45–60°N displayed in Figure 5b shows clearly less persistence of ozone anomalies (see also Figure 3b). This is confirmed by a low first eigenvalue (7.28) which accounts only for 60.1% of the variance of the underlying data set. Comparing the first eigenvalues for the two different latitude bands thus confirms the conclusions from Figures 3 and 5.

[24] While the magnitude of the first eigenvalue indicates how much of the variance of the whole underlying data set is explained by the first principal component, it does not show how well each individual time series of ozone anomalies of the underlying data set is explained by the first principal component. A way to quantify the latter is to calculate the corresponding correlation coefficients between these two quantities. Figure 6 (orange line) shows these correlation coefficients (which are also called the factor loading) for the corresponding data set from Figure 5a. The first principal component is strongly correlated with the ozone anomalies for each individual month within the time frame with correlation coefficients higher than 0.9, except for the correlation coefficient for October which is 0.7. Furthermore Figure 6 (blue line) displays the factor loading for the midlatitude band 45–60°N from Figure 5b, which shows clearly less persistence of ozone anomalies. The factor loading reveals that this is mainly due to the ozone anomalies from October to January, which show small correlation coefficients with the first principal component. The loadings on the remaining months of the year are high with correlation coefficients greater than 0.9 after March. Figure 6 shows in addition the correlation coefficients

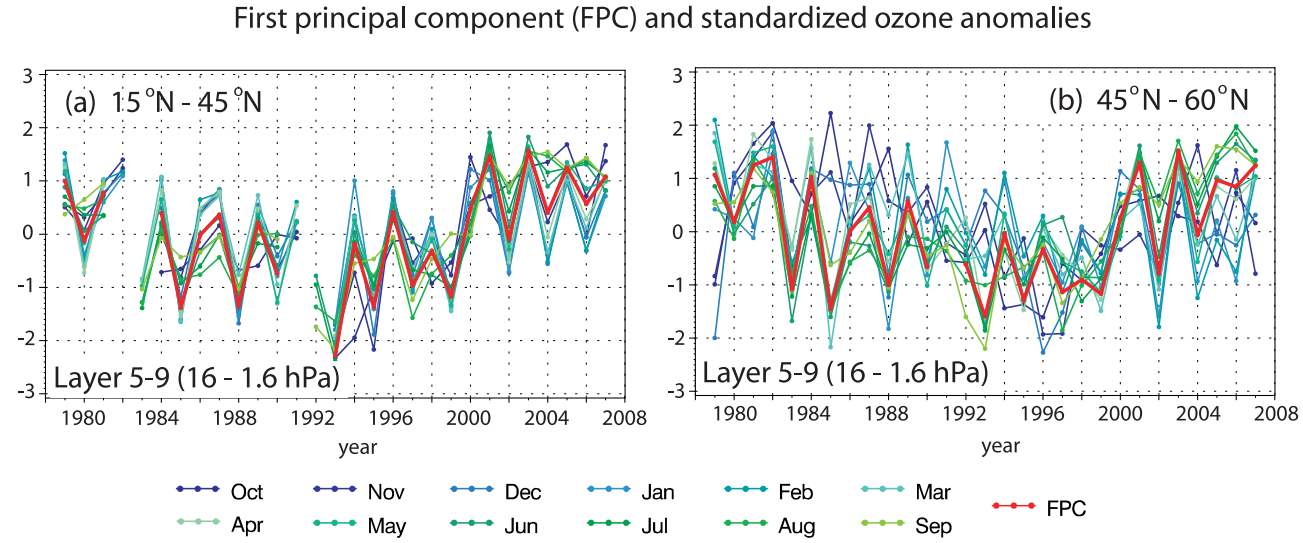

Figure 5. Detrended standardized ozone anomalies for the different months of the time frame starting in October and ending in September of the following year in the upper layers of the merged SBUV(/2) profile ozone data for (a) 15–45°N and (b) 45–60°N. The corresponding first principal components for the two data sets are displayed as red lines.

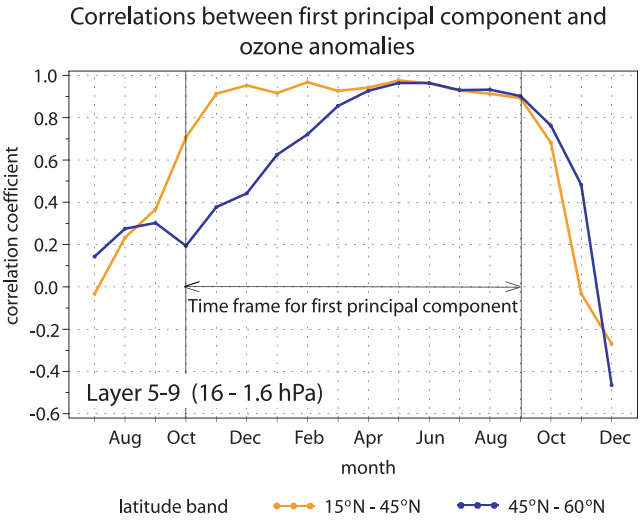

Figure 6. Correlation coefficients between the first principal component for SBUV(/2) upper stratospheric ozone anomalies from October to September of the following year and the ozone anomalies in the individual months. Coefficients are shown for the latitude band 15–45°N (orange line) and 45–60°N (blue line).

between the first principal component and the ozone anomalies in the 3 months preceding and following the chosen time frame. The coefficients are small, illustrating the fact that the persistence does not exceed the time frame from autumn to autumn of the following year.

[25] By choosing the structure of the underlying matrix the time frame of the analyzed correlations is defined. In the above, the time frame from October to September of the following year was examined. In the same way it is possible to analyze other time frames, e.g., from November to October of the following year. In this case it is assumed that the ozone anomalies in October belong to the cluster that ends in October instead of to the cluster that starts in October. The strength of ozone autocorrelation functions within different time frames can be examined on the basis of the first eigenvalue. The higher its value, the more variance can be explained by a single component and the more persistence in ozone anomalies can be found for that time frame.

[26] Thus, the first eigenvalue can be used to study the strength of the autocorrelation functions for varying latitude regions, altitude regions and time frames. Figure 7 displays 12 panels which correspond to the combinations of three altitude regions (1000–1.6 hPa, 1000–16 hPa, and 16–1.6 hPa) and four time frames (September–August, October–September, November–October, and December–November). Each dot in such a panel represents the first eigenvalue for a certain latitude bin which is denoted by the lower and upper latitude borders given on the x and y axes. For all three altitude regions the largest eigenvalues can be found for the time frames starting in October and November. Therefore the persistence of ozone anomalies starts in October/November and ends in September/October of the following year.

[27] We focus on Figure 7b, showing the time frame October–September. The eigenvalues take very high values in the upper stratosphere (Figure 7b, third panel) for all the regions varying between 10–50°N (marked with an ellipse). The highest eigenvalue, with a magnitude of 10.18, is found for the latitude band 15–40°N. In this region, the fraction of variance of the 12 time series of ozone anomalies explained by the first principal component is equal to 0.85. The correlations in the upper stratosphere are much higher than for the corresponding regions in the lower stratosphere (Figure 7b, second panel) or the total ozone column (Figure 7b, first panel), which is confirmed by the example for the region 15–45°N shown in Figure 3. In the lower stratosphere, the highest correlations can be found for all the regions varying between 30 and 60°N (marked with an ellipse). However, they are clearly less strong than the patterns between 10 and 50°N in the upper stratosphere. The regions between 30 and 60°N are the only latitude bins where the correlations in the lower stratosphere are stronger than the corresponding correlations in the upper stratosphere. The persistence of total ozone anomalies (Figure 7b, first panel) for the October–September time frame peaks in the subtropical region (ellipse on the left side) and in the midlatitudes (ellipse on the right side) and is therefore a result of the persistence in both the lower and upper stratospheric anomalies.

4. Persistence of Upper Stratospheric Anomalies in Other Trace Species

[28] Using the techniques of autocorrelation functions and PCA we have identified two regions with strong seasonal persistence of ozone anomalies. One region is the midlatitude (30–60°N) lower stratosphere, where the anomalies established during winter from the transport of ozone itself can persist because of the long lifetime of O_x in this region. This ozone memory in the lower stratosphere causes the strong memory in the total ozone column which was identified by FS 2003. The second region with an even stronger seasonal persistence of ozone anomalies is the subtropical and midlatitude (10–50°N) upper stratosphere (16–1.6 hPa). Because of the short lifetime of O_x in this region, it is not possible for the memory to reside in the ozone itself, as in the lower stratosphere. Rather, it must come from something else.

[29] Anomalies of the photochemically controlled upper stratospheric ozone could result from temperature anomalies, which have an effect on reaction rates and therefore influence the chemical destruction of odd oxygen. However, there is not a great deal of dynamical variability in the late spring and summer stratosphere at midlatitudes, and the radiative timescale is much too short for temperature anomalies in winter and early spring to persist until summer.

Figure 7. First eigenvalues for correlation matrices corresponding to underlying matrices of ozone anomalies for the time frames (a) September to August, (b) October to September, (c) November to October, and (d) December to November. Each dot corresponds to the first eigenvalue for a certain latitude bin which is denoted by the lower and upper latitude boundaries given on the x and y axes. Values below 6.8 are not shown.

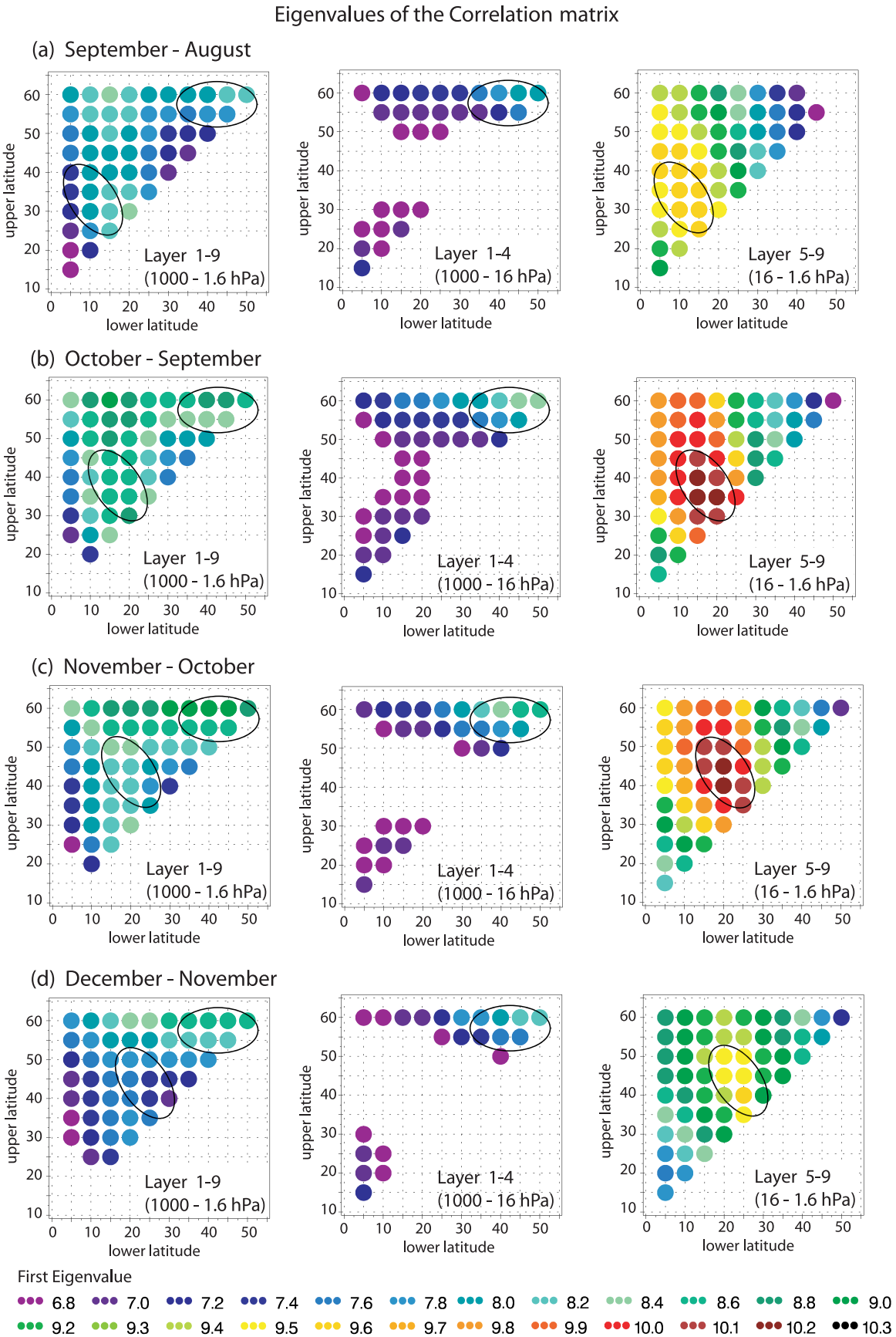
Eigenvalues of the Correlation matrix
(a) September - August
(b) October - September
(c) November - October
(d) December - November
upper latitude
lower latitude
Layer 1-9
(1000 - 1.6 hPa)
Layer 1-4
(1000 - 16 hPa)
Layer 5-9
(16 - 1.6 hPa)
First Eigenvalue
6.8 7.0 7.2 7.4 7.6 7.8 8.0 8.2 8.4 8.6 8.8 9.0
9.2 9.3 9.4 9.5 9.6 9.7 9.8 9.9 10.0 10.1 10.2 10.3

Figure 7

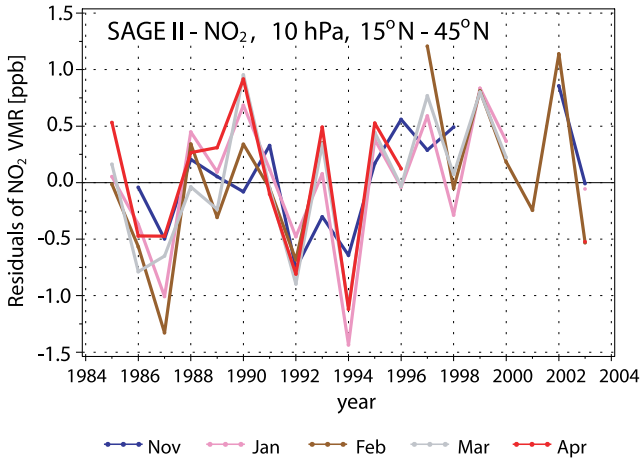

Figure 8. Time series of NO_2 anomalies averaged over 15–45°N at 10 hPa for the 5 months November, January, February, March, and April for SAGE II sunset measurements.

Indeed, autocorrelation functions for stratospheric temperature do not show any signs of a clustered structure (not shown). Hence, there is no seasonal persistence in the upper stratospheric temperature from the autumn of one year until the autumn of the following year that could cause the observed persistence of ozone anomalies. This suggests that the seasonal persistence of upper stratospheric ozone anomalies must arise from a different mechanism.

[30] As discussed in the Introduction, the winter-spring upper stratospheric extratropical ozone anomalies that are coherent with the QBO have been attributed to NO_2 anomalies induced by the effect of the QBO on the dynamical forcing of the Brewer-Dobson circulation [*Zawodny and McCormick*, 1991; *Chipperfield et al.*, 1994]. The possibility of transport-induced extratropical wintertime NO_2 anomalies is not specific to the QBO, of course, and would arise from any dynamical variability of the Brewer-Dobson circulation whatever its cause. Since NO_y (the total reactive nitrogen reservoir) has a long lifetime (exceeding 1 year for 30–40 km [*Brasseur and Solomon*, 1984]) we hypothesize that transport-induced NO_y (and hence NO_2) anomalies persist through the autumn to autumn time frame, and that this is the mechanism responsible for the seasonal persistence of the upper stratospheric ozone anomalies. Note that this mechanism is consistent with the observation made concerning Figure 1c that the upper stratospheric ozone anomalies do not appear to decay in magnitude during the dynamically quiescent summer, since we would not expect the NO_y anomalies to appreciably decay.

[31] In order to test this hypothesis we investigate the persistence of NO_2 anomalies in the same region. Figure 8 shows the year to year variability of the SAGE II NO_2 anomalies averaged over 15–45°N at 10 hPa for 5 months. The individual months in the SAGE II NO_2 data set show quite substantial data gaps for a number of years and we only show the months with adequate data coverage: November, January, February, March, and April. The interannual NO_2 anomalies do not change their magnitude (which corresponds to 25% of the absolute values) during the months shown here and are clearly correlated from month to month. This is confirmed by the very high correlation coefficients between the time series for the different months, given in Table 2. The correlations between November and the other months are not quite as strong as the correlations later in winter since November is a transitional month during which the anomalies of one year change to the anomalies of the next year. The number of data points which are available to calculate the correlation coefficients are given in parentheses beside the corresponding coefficients. Note that the number of data points is quite small for some coefficients, e.g., the number of years where NO_2 values are available for both March and April is 11. (For 11 data points, correlation coefficients need to be larger than 0.61 to be statistically significant at the 95% confidence level.) However, both the correlation coefficients (Table 2) and the picture of the time series (Figure 8) illustrate clearly that NO_2 anomalies persist from late autumn until spring.

Table 2. Correlation Coefficients Between Monthly Mean SAGE II NO_2 Anomalies Averaged Over 15–45°N at 10 hPa[a]

	November	January	February	March	April
November	1 (15)	0.61 (14)	0.68 (12)	0.56 (13)	0.56 (12)
January		1 (17)	0.90 (14)	0.88 (16)	0.86 (13)
February			1 (16)	0.87 (13)	0.80 (11)
March				1 (16)	0.96 (11)
April					1 (13)

[a]The number of data points which are available to calculate the correlation coefficients are given in parentheses beside the corresponding coefficients.

[32] Unfortunately because of substantial gaps in the SAGE II NO_2 data set we cannot analyze the behavior of the NO_2 persistence after April. To further investigate this issue we look into HALOE NO_x measurements. Figure 9 shows the year to year variability of HALOE NO_x anomalies averaged over 15–45° equivalent latitude at 10 hPa for the 10 months from December to September of the following year. The individual months show some data gaps for a number of years. In general the number of years is too small to calculate meaningful correlation coefficients between the time series. However, the NO_x anomalies clearly persist

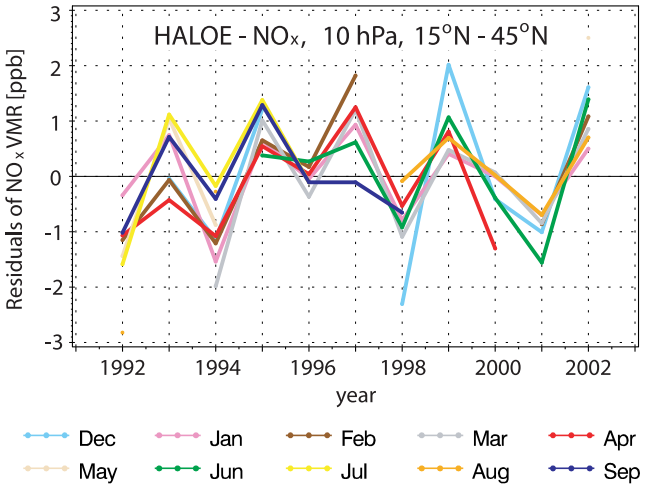

Figure 9. Time series of NO_x anomalies averaged over 15–45° equivalent latitude at 10 hPa for HALOE. The 10 months from December until September of the following year are shown.

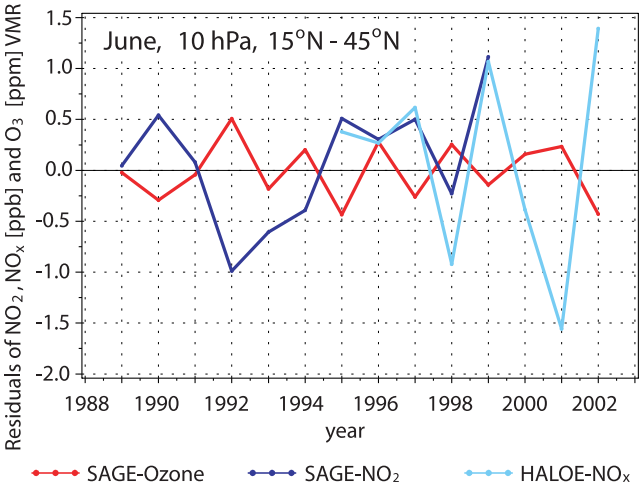

Figure 10. Time series of SAGE II ozone (red), SAGE II NO_2 (dark blue), and HALOE NO_x (light blue) June anomalies averaged over 15–45°N (15–45° equivalent latitude for HALOE) at 10 hPa.

from winter through spring and summer until the following autumn. This strengthens our hypothesis that the persistence of NO_2 anomalies extends through late spring and summer. The indication of the NO_2 anomaly persistence on the one hand, and the instantaneous winter/spring correlations (found in previous studies) between ozone and NO_2 on the other hand, points to the mechanism of transport-induced NO_y anomalies and their seasonal persistence causing the observed persistence of upper stratospheric ozone anomalies. It furthermore provides an explanation for the observed year-to-year summertime ozone variability in the upper stratosphere.

[33] An additional test of our hypothesis would be to confirm that upper stratospheric ozone and NO_2 anomalies are negatively correlated during the summer. Our data are in agreement with previous results in that we find a strong anticorrelation between SAGE II ozone and NO_2 in winter and spring when the QBO signal in the two trace gases is strong (e.g., a correlation coefficient of −0.78 in January based on 17 data points). Unfortunately, as noted above only very limited NO_2 data is available for the summer months. Figure 10 shows the June anomalies of SAGE II ozone, SAGE II NO_2 and HALOE NO_x from 1989 through 2002 averaged over 15–45°N (15–45° equivalent latitude for HALOE) at 10 hPa. Although the record is too short to draw a definitive conclusion, the available evidence is at least consistent with our hypothesis: a negative correlation between ozone and NO_2/NO_x is suggested by Figure 10, and the correlation coefficient between SAGE II ozone and NO_2 is -0.64, which for 11 data points is (just) significant at the 95% confidence level.

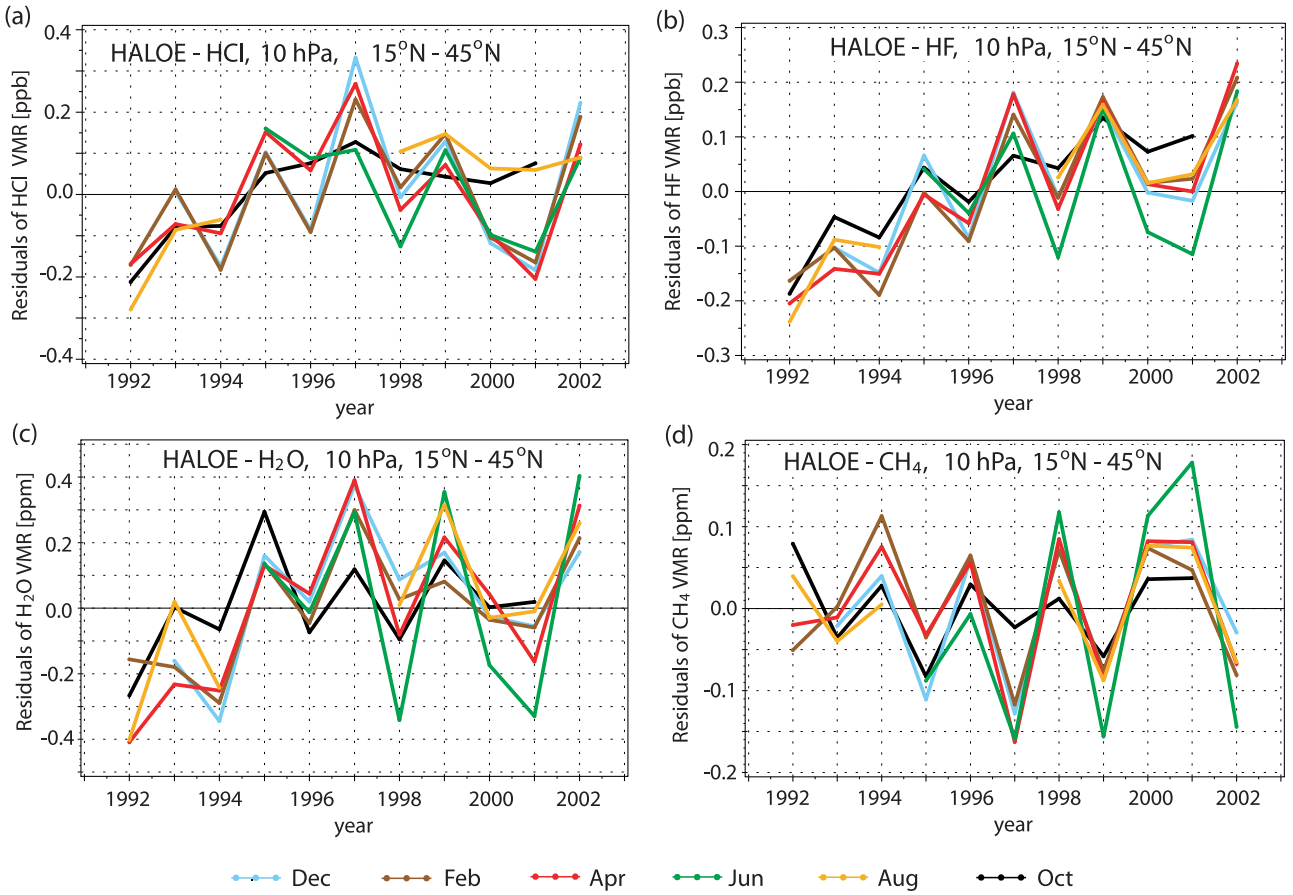

Figure 11. Time series of (a) HCl, (b) HF, (c) H_2O, and (d) CH_4 anomalies averaged over 15–45° equivalent latitude at 10 hPa for HALOE. Every second month from December until October of the following year is shown.

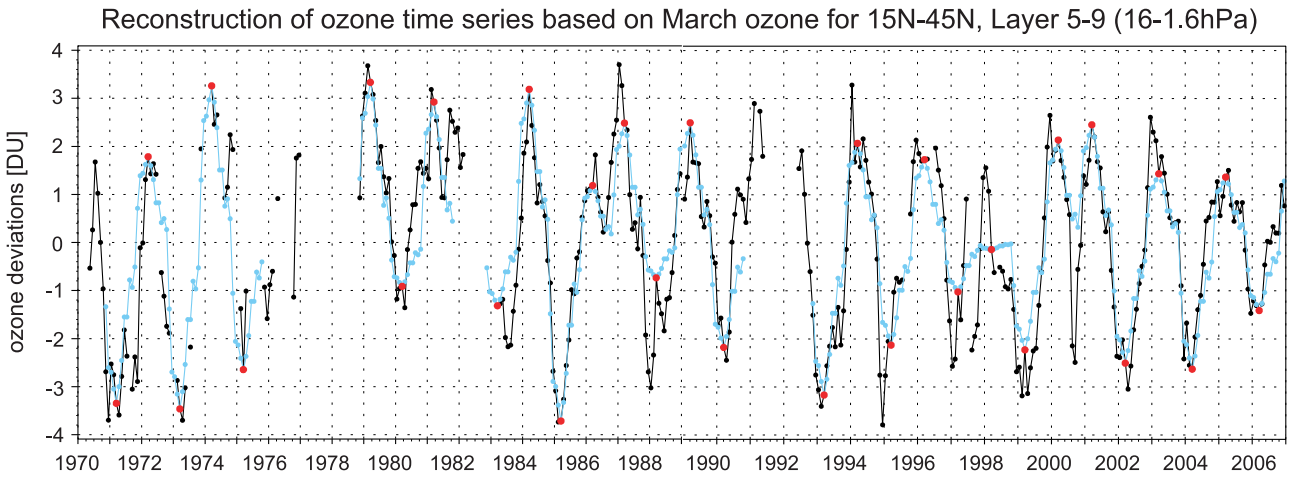

Figure 12. Time series of ozone anomalies averaged over 15–45°N between 16 and 1.6 hPa for the merged SBUV(/2) data set (black) and from a reconstruction (blue) based on March ozone (red) and the correlation coefficients between ozone in March and ozone in the other months. The correlation coefficient between the original time series and the reconstructed time series is 0.88.

[34] As a final test, if our hypothesis is true then we would expect to see the same seasonal persistence of anomalies of other trace gases in the extratropical upper stratosphere. Figure 11 shows the year to year variability of HALOE HCl, HF, H_2O and CH_4 anomalies averaged over 15–45° equivalent latitude at 10 hPa. For clarity only every second month of the time period from December until October of the following year is displayed. For all four trace gases the anomalies establish during late autumn/early winter and then persist through the whole spring and summer. In October the magnitude of the anomalies decreases and November (not shown here) is a transitional month where the anomalies of the next winter start to build up. Long-lived trace gases in the upper stratosphere are therefore generally characterized by the seasonal persistence of their interannual anomalies. Moreover the sign of the anomalies is related to that of NO_y in the way one would expect from the variations in age of air that arise from variations in the dynamical forcing of the Brewer-Dobson circulation, e.g., high NO_y is associated with high H_2O and low CH_4.

5. Summary and Discussion

[35] Analysis of ozone profile data in the Northern Hemisphere has demonstrated that lower stratospheric anomalies persist from November to October of the following year. This seasonal persistence is particularly strong in the 45–60°N latitudinal belt. In the upper stratosphere, an even stronger persistence of ozone anomalies from November to October was found over 15–45°N.

[36] Year to year variability of ozone in the extratropical upper stratosphere is known to be dominated by the QBO during winter and early spring. This study suggests that the QBO signal in this region is not just a modulation of the QBO cycle by the annual cycle. The equatorial winds in late autumn–early winter affect the stratospheric circulation and therefore affect ozone anomalies through winter into early spring. These anomalies persist through the entire year up to the next October.

[37] The mechanism responsible for persistence of ozone anomalies in the lower stratosphere is related to ozone build-up in winter-spring with the subsequent (slow) summertime photochemical relaxation of ozone. This mechanism cannot explain the persistence of ozone anomalies in the upper stratosphere, as there the O_x lifetime is too short to allow the persistence of transport-induced ozone anomalies. However, a plausible mechanism is the persistence of transport-induced wintertime anomalies in NO_y, which would perturb ozone through NO_x chemistry. Transport-induced wintertime anomalies in NO_y arise from variations in the dynamical forcing of the Brewer-Dobson circulation, which make the air at a given location either anomalously young (with low NO_y) or old (with high NO_y). (The QBO is one, but not the only, mechanism for such variations.) Although the available observations are limited, we show that there is compelling evidence for the seasonal persistence of NO_2 (and NO_x) anomalies. Further evidence for this mechanism is provided by the analysis of other long-lived trace gases, which show the same seasonal persistence of interannual anomalies.

[38] Strictly speaking, we cannot prove that the summertime upper stratospheric extratropical ozone anomalies are caused by the NO_2 anomalies. For that we rely on the detailed modeling studies cited earlier which have attributed winter-spring upper stratospheric QBO ozone anomalies to NO_2 anomalies, and on the fact that NO_x is by far the dominant catalytic ozone destroyer in the region in question, 30–40 km [*Brasseur and Solomon*, 1984]. However, it is quite true that all long-lived species involved in catalytic ozone destruction (Cl_y, Br_y, H_2O) would exhibit transport-induced winter-spring variations which would persist through summer. So, in principle, our proposed mechanism for summertime persistence of ozone anomalies could involve contributions from all catalytic species.

[39] One practical application of ozone anomaly persistence in the upper stratosphere is that ozone values in late spring, summer, and autumn can be predicted already in winter and early spring. This is demonstrated in Figure 12 for the SBUV(/2) time series of ozone anomalies averaged

over 15–45°N between 16 and 1.6 hPa. The ozone time series from 1970 to 2007 is shown as a black line and the March ozone values of this time series are highlighted as red dots. SBUV data after August 2000 are based on the NOAA 16 instrument. For Figure 12 a bias of approximately 2% between the NOAA 16 instrument and previous SBUV instruments has been removed using a statistical ''intervention'' technique [e.g., *Reinsel et al.*, 1994]. The blue line in Figure 12 shows a reconstruction of the original time series which is based on the March ozone values and the correlation coefficients between ozone in March and ozone in the other months. The reconstructed time series is seen to capture very well all the features of the original time series; the correlation coefficient between them is extremely high (0.88). For nearly all the years the full seasonal cycle of the ozone deviations can be reconstructed on the basis of just a single value for that year. Moreover the interannual variability of the reconstructed time series is in very good agreement with the interannual variability of the original time series. The prediction capabilities that we see here are highly seasonal: with the approach used in Figure 12 it is possible to predict the September ozone deviation 9 months ahead on the basis of the values in the previous December, but December values cannot be accurately predicted from the previous September values which are just 3 months away. This shows that seasonal persistence is a completely distinct phenomenon from dependence on some slowly varying external factor such as the QBO.

[40] Figure 12 demonstrates that for a year with a given ozone value in March but missing ozone values for the subsequent months (e.g., 1972 and 1973) we are able to fill such data gaps with our method (at least over 15–45°N between 16 and 1.6 hPa). Since most of the ozone variability can be described by just one principal component, this component can be estimated from available data (or, perhaps, a model) and then used to reconstruct the missing data. This is particularly important for records of satellite ozone profile measurements by the occultation method (e.g., SAGE), for which the measurements are sparse and there are months with no measurements over wide latitudinal belts. This method of filling data gaps captures the seasonality of the ozone deviations. Previous studies which link equatorial winds with midlatitude ozone deviations using regression methods [*Randel and Cobb*, 1994; *Randel and Wu*, 1996, 2007] show good results in winter-spring, when prediction capabilities are high for several adjacent months because of a slowly changing QBO-related signal. However, these methods do not capture the seasonality of the ozone correlations and would be less useful in summer and autumn, when the correlation between the equatorial wind and extratropical ozone is small [*Randel and Wu*, 2007]. Nor can one simply interpolate between early autumn and late autumn because the memory of the interannual anomalies is lost during this period.

[41] The prediction capabilities can be used as a validation diagnostic for chemistry climate models [*Tegtmeier and Shepherd*, 2007]. They also may be useful for comparing ozone values obtained in different months for the purpose of data validation. The same remarks apply in principle to other species for which there is a strong seasonal persistence of interannual anomalies, but for species other than ozone the data records are not yet long enough to establish reliable estimates of the correlation coefficients.

[42] **Acknowledgments.** The authors are grateful to R. Stolarski, S. Hollandsworth Frith, and their colleagues from NASA Goddard Space Flight Center for making the merged SBUV data sets available. The authors also would like to thank the NASA Langley Research Center (NASA-LaRC) for making SAGE II and HALOE data available. We thank Ralph Lehmann from AWI for helpful discussions. S.T. especially acknowledges the Canadian Natural Sciences and Engineering Research Council postdoctoral fellowship allowing this study to be completed. T.G.S. is supported by the Natural Sciences and Engineering Research Council, the Canadian Foundation for Climate and Atmospheric Sciences, and the Canadian Space Agency.

References

Afifi, A. A., and S. P. Azen (1979), *Statistical Analysis: A Computer-Oriented Approach*, 2nd ed., Academic, New York.

Bhartia, P. K., C. G. Wellemeyer, S. L. Taylor, N. Nath, and A. Gopolan (2004), Solar backscatter ultraviolet (SBUV) version 8 profile algorithm, paper presented at Quadrennial Ozone Symposium, Int. Ozone Comm., Kos, Greece.

Brasseur, G., and S. Solomon (1984), *Aeronomy of the Middle Atmosphere*, Reidel, D., Dordrecht, Netherlands.

Chipperfield, M. P., L. J. Gray, J. S. Kinnersley, and J. Zawodny (1994), A two-dimensional model study of the QBO signal in SAGE II NO_2 and O_3, *Geophys. Res. Lett.*, *21*, 589–592, doi:10.1029/94GL00211.

Fioletov, V. E., and T. G. Shepherd (2003), Seasonal persistence of midlatitude total ozone anomalies, *Geophys. Res. Lett.*, *30*(7), 1417, doi:10.1029/2002GL016739.

Fioletov, V. E., and T. G. Shepherd (2005), Summertime total ozone variations over middle and polar latitudes, *Geophys. Res. Lett.*, *32*, L04807, doi:10.1029/2004GL022080.

Fioletov, V. E., D. W. Tarasick, and I. Petropavlovskikh (2006), Estimating ozone variability and instrument uncertainties from SBUV (/2), ozonesonde, Umkehr, and SAGE II measurements: Short-term variations, *J. Geophys. Res.*, *111*, D02305, doi:10.1029/2005JD006340.

Frith, S., and R. S. Stolarski (2005), Merged profile ozone data from the SBUV/SBUV2 series of instruments, *Eos Trans. AGU*, *86*(52), Fall Meet. Suppl., Abstract A23B-0943.

Fusco, A. C., and M. L. Salby (1999), Interannual variations of total ozone and their relationship to variations of planetary wave activity, *J. Clim.*, *12*, 1619–1629.

Gray, L. J., and T. J. Dunkerton (1990), Seasonal cycle modulations of the equatorial QBO, *J. Atmos. Sci.*, *47*, 2429–2451, doi:10.1175/1520-0469(1990)047<2429:TROTSC>2.0.CO;2.

Grooβ, J.-U., and J. M. Russell III (2005), Technical note: A stratospheric climatology for O_3, H_2O, CH_4, NO_x, HCl and HF derived from HALOE measurements, *Atmos. Chem. Phys.*, *5*, 2797–2807.

Hamilton, K. (1989), Interhemispheric asymmetry and annual synchronization of the ozone quasi-biennial oscillation, *J. Atmos. Sci.*, *46*, 1019–1025, doi:10.1175/1520-0469(1989)046<1019:IAAASO>2.0.CO;2.

Holton, J. R., and H.-C. Tan (1980), The influence of the equatorial quasi-biennial oscillation on the global circulation at 50 mb, *J. Atmos. Sci.*, *37*, 2200–2208, doi:10.1175/1520-0469(1980)037<2200:TIOTEQ>2.0.CO;2.

McCormick, M. P., J. M. Zawodny, R. E. Veiga, J. C. Larsen, and P.-H. Wang (1989), An overview of SAGE I and II ozone measurements, *Planet. Space Sci.*, *37*, 1567–1586, doi:10.1016/0032-0633(89)90146-3.

Nazaryan, H., and M. P. McCormick (2005), Comparisons of Stratospheric Aerosol and Gas Experiment (SAGE II) and Solar Backscatter Ultraviolet Instrument (SBUV/2) ozone profiles and trend estimates, *J. Geophys. Res.*, *110*, D17302, doi:10.1029/2004JD005483.

Newman, P. A., J. S. Daniel, D. W. Waugh, and E. R. Nash (2007), A new formulation of equivalent effective stratospheric chlorine (EESC), *Atmos. Chem. Phys.*, *7*, 4537–4552.

Petropavlovskikh, I., C. Ahn, P. K. Bhartia, and L. E. Flynn (2005), Comparison and covalidation of ozone anomalies and variability observed in SBUV (/2) and Umkehr northern midlatitude ozone profile estimates, *Geophys. Res. Lett.*, *32*, L06805, doi:10.1029/2004GL022002.

Preisendorfer, R. W. (1988), *Principal Component Analysis in Meteorology and Oceanography*, 425 pp., Elsevier, Amsterdam.

Randel, W. J., and J. B. Cobb (1994), Coherent variations of monthly mean column ozone and lower stratospheric temperature, *J. Geophys. Res.*, *99*, 5433–5447, doi:10.1029/93JD03454.

Randel, W. J., and F. Wu (1995), Climatology of stratospheric ozone based on SBUV and SBUV/2 data: 1978–1994, *NCAR Tech. Note, NCRA/TN-412+STR*, Natl. Cent. for Atmos. Res., Boulder, Colo.

Randel, W. J., and F. Wu (1996), Isolation of the ozone QBO in SAGE II data by singular value decomposition, *J. Atmos. Sci.*, *53*, 2546–2559, doi:10.1175/1520-0469(1996)053<2546:IOTOQI>2.0.CO;2.

Randel, W. J., and F. Wu (2007), A stratospheric ozone profile data set for 1979–2005: Variability, trends, and comparisons with column ozone data, *J. Geophys. Res.*, *112*, D06313, doi:10.1029/2006JD007339.

Randel, W. J., F. Wu, and R. Stolarski (2002), Changes in column ozone correlated with the stratospheric EP flux, *J. Meteorol. Soc. Jpn.*, *80*, 849–862, doi:10.2151/jmsj.80.849.

Reinsel, G. C., G. C. Tiao, D. J. Wuebbles, J. B. Kerr, A. J. Miller, R. M. Nagatani, L. Bishop, and L. H. Ying (1994), Seasonal trend analysis of published ground-based and TOMS total ozone data through 1991, *J. Geophys. Res.*, *99*, 5449–5464, doi:10.1029/93JD03517.

Richman, M. B. (1986), Rotation of principal components, *J. Climatol.*, *6*, 293–335, doi:10.1002/joc.3370060305.

Rind, D., J. Lerner, and J. Zawodny (2005), A complementary analysis for SAGE II data profiles, *Geophys. Res. Lett.*, *32*, L07812, doi:10.1029/2005GL022550.

Russell, J. M., III, L. L. Gordley, J. H. Park, S. R. Drayson, D. H. Hesketh, R. J. Cicerone, A. F. Tuck, J. E. Frederick, J. E. Harries, and P. J. Crutzen (1993), The Halogen Occultation Experiment, *J. Geophys. Res.*, *98*, 10,777–10,797, doi:10.1029/93JD00799.

Tegtmeier, S., and T. G. Shepherd (2007), Persistence and photochemical decay of springtime total ozone anomalies in the Canadian Middle Atmosphere Model, *Atmos. Chem. Phys.*, *7*, 485–493.

Terao, Y., and J. A. Logan (2007), Consistency of time series and trends of stratospheric ozone as seen by ozonesonde, SAGE II, HALOE, and SBUV (/2), *J. Geophys. Res.*, *112*, D06310, doi:10.1029/2006JD007667.

Tian, W., M. P. Chipperfield, L. J. Gray, and J. M. Zawodny (2006), Quasi-biennial oscillation and tracer distributions in a coupled chemistry-climate model, *J. Geophys. Res.*, *111*, D20301, doi:10.1029/2005JD006871.

Tung, K. K., and H. Yang (1994), Global QBO in circulation and ozone. Part I: Reexamination of observational evidence, *J. Atmos. Sci.*, *51*, 2699–2707, doi:10.1175/1520-0469(1994)051<2699:GQICAO>2.0.CO;2.

Weber, M., S. Dhomse, F. Wittrock, A. Richter, B. Sinnhuber, and J. P. Burrows (2003), Dynamical control of NH and SH winter/spring total ozone from GOME observations in 1995–2002, *Geophys. Res. Lett.*, *30*(11), 1583, doi:10.1029/2002GL016799.

Zawodny, J. M., and M. P. McCormick (1991), Stratospheric Aerosol and Gas Experiment II measurements of the quasi-biennial oscillations in ozone and nitrogen dioxide, *J. Geophys. Res.*, *96*, 9371–9377, doi:10.1029/91JD00517.

V. E. Fioletov and S. Tegtmeier, Environment Canada, Toronto, ON M3H 5T4, Canada. (susann@atmosp.physics.utoronto.ca)

T. G. Shepherd, Department of Physics, University of Toronto, Toronto, ON M5S 1A7, Canada.